ELSEVIER

International Journal of Heat and Fluid Flow 23 (2002) 205–219

International Journal of HEAT AND FLUID FLOW

www.elsevier.com/locate/ijhff

Investigation of the flow field of a highly heated jet of air

Susan M. Anderson *, Klaus Bremhorst

Department of Mechanical Engineering, The University of Queensland, Brisbane, Qld 4072, Australia

Abstract

Measurements of mean and fluctuating velocity and temperature and their self- and cross-products to the third-order are presented for a heated axisymmetric air jet. Froude numbers in the range of 3500–13,190, Reynolds numbers in the range of 3470–8500 and non-dimensional streamwise distances, X^*, from 0.27 to 1.98 are covered by the data. It was found that turbulence intensity decreases for the heated jet in the region between the inertia dominated and the buoyancy dominated regions which is contrary to findings with helium jets mixing with ambient air to produce density fluctuations. The effects of heating on the turbulent kinetic energy budget and the temperature variance budget show small differences for the inertia dominated region and the intermediate region which help to explain the transition process to the far field plume region. Constants are evaluated for the isotropic eddy diffusivity and generalised gradient hypothesis models as well as the scalar variance model. No significant effect of heating on the dissipation time-scale ratio was found. A novel wire array with an inclined cold wire was used. Measurements obtained with this probe are found to lead to asymmetries in some of the higher-order products. Further investigation suggested that the asymmetries are attributable to an as yet unreported interference effect produced by the leading prong of the inclined temperature wire. The effect may also have implications for inclined velocity wires which contain a temperature component when used in heated flows.

Keywords: Heated axisymmetric jet; Variable density jet; Hot wire anemometer; Cold wire anemometer; Dissipation time-scale ratio; Diffusivity and scalar variance model constants

1. Introduction

Fluid density changes can be brought about by mixing of fluids of different density or by heating the fluid so that temperature changes influence fluid density. Density can also be affected by chemical reactions or by increasing the flow Mach number in order to introduce pressure changes, but such flows are outside the scope of the present study. The effect of changes to the flow induced by changing density is of interest for prediction of flows in engineering design. Based on Morkovin's hypothesis, it is assumed that the effect of density fluctuations on turbulence structure is small so that only the effect of mean density changes need be included in computation of variable density flow fields (cf. Morkovin, 1962). While this has led to considerable success in the simulation of low and high speed flows, it does not explain the exact nature of density effects on the flow physics or structural changes, if any.

It is of particular interest what effect density changes have on the turbulent energy flows in the transition from inertia dominated flow to one dominated by buoyancy and whether the way in which density changes are produced, leads to different mechanisms. For example, is the flow structure for a variable density jet produced by mixing of two incompressible fluids of different density the same as that in a jet where density changes are produced by heating. Both jets produce the same effect on the mean motion of the flow because they both produce the same mean density profiles (Chen and Rodi, 1980) but this does not give information on the structural changes within the jet.

Chen and Rodi (1980) in their comprehensive survey of turbulent buoyant jets, derived decay laws for mean velocity and density over the regions of the jet, based on the exit Froude number defined by Eq. (1)

$$Fr = \frac{\bar{U}_{ex}^2 \bar{\rho}_{ex}}{gd(\rho_{amb} - \bar{\rho}_{ex})}. \quad (1)$$

* Corresponding author. Tel.: +61-7-3365-3588; fax: +61-7-3365-4799.

E-mail address: anderson@mech.uq.edu.au (S.M. Anderson).

0142-727X/02/$ - see front matter
PII: S0142-727X(01)00150-3

Nomenclature

C_μ, C_θ, C_t	constants
d	nozzle exit diameter (mm)
Fr	Froude number
g	acceleration of gravity (m/s^2)
g^*	non-dimensional excess density
k	turbulent kinetic energy (m^2/s^2)
p	fluid pressure fluctuation (Pa)
$\bar{P}$	mean fluid pressure (Pa)
r	coordinate normal to jet axis (mm)
R	time-scale ratio, gas constant or correlation coefficient
t	temperature fluctuation (K)
T	absolute temperature (K)
u	velocity or streamwise velocity fluctuation (m/s)
U	instantaneous streamwise velocity (m/s)
U^*	non-dimensional streamwise velocity
v	radial velocity fluctuation (m/s)
V	instantaneous radial velocity (m/s)
w	azimuthal velocity fluctuation (m/s)
x	streamwise coordinate (mm)
X^*	non-dimensional streamwise distance
y	variable

Greeks

Δ	difference
ε	dissipation rate (m^2/s^3)
v_θ	eddy diffusivity of heat (m^2/s)
ρ	density (m^3/kg)
σ_t	turbulent Prandtl number

Superscripts

$\bar{}$	time average
$'$	fluctuation
$''$	density weighted fluctuation
$\tilde{}$	Favre averaged mean

Subscripts

0.5	half-value relative to centreline
amb	ambient
c/line	centreline
ex	exit
f	Favre averaged
HW	hot wire
i, j	tensor indices
k	based on kinetic energy
rms	root mean square value
$\widetilde{t''^2}$	based on Favre averaged temperature variance

Self-similarity has been shown to exist in the two extreme regions of a buoyant jet – the initial variable density, inertia dominated region near the jet exit and in the far field buoyancy dominated region where the jet behaves like a plume. Demarcation of the three regions of a buoyant jet have been expressed in terms of the dimensionless downstream distance parameter X^*, Eq. (2), where x is the axial distance from the jet exit. $0 < X^* \leqslant 0.5$ is the inertia dominated region, $X^* > 5$ the plume region and the transition region spans the intermediate region between these two.

$$X^* = Fr^{-1/2}\left(\frac{\bar{\rho}_{ex}}{\rho_{amb}}\right)^{-1/4}\frac{x}{d}. \tag{2}$$

However, Peterson and Bayazitoglu (1992) found their mean velocity decay data in the intermediate region fitted an equation slightly different to Chen and Rodi's (1980) while Amielh et al. (1996) found the equation derived by Chen and Rodi (1980) fitted their helium jet data well. Ogino et al.'s (1980) measurements in a heated water jet showed that $X^* = 1$ was a more appropriate delineation of the inertia dominated region for the mean velocity data.

From the above, it is seen that the behaviour of a jet does not neatly fall into the three regions identified by Chen and Rodi (1980). There are no clear lines separating the regions, and the intermediate region spans a distance at least 10 times the length of the non-buoyant region, regardless of exit Froude number.

Numerous data sets exist for the inertia dominated region of the jet, Corrsin and Uberoi (1949), Wilson and Danckwerts (1964), Chevray and Tutu (1978), Antonia et al. (1975), Bashir and Uberoi (1975), Antonia et al. (1983), Lockwood and Moneib (1980), and Chua and Antonia (1990).

Peterson and Bayazitoglu (1992) measured only mean and turbulent velocity data in the three regions of a heated axisymmetric air jet at Reynolds numbers of 500–7500, using a laser Doppler anemometer (hence there is no temperature data available). Selected half-profiles of $\bar{U}, u_{rms}$ and $\overline{uv}$ were presented in the intermediate region of their heated jet and a decrease in turbulence intensity was noted in this region. Turbulence intensities were 10–15% lower than in the unheated jet. The reason proposed for the obvious difference in $\overline{uv}$ and u_{rms} was attributed to the effect of buoyancy. The exact mechanism is, however, unknown. Overall, results indicated that significant errors would result if turbulence models did not consider the variation in these correlations. No other turbulence measurements in the intermediate region of heated air jets have been reported for comparison.

Panchapakesan and Lumley (1993), compared measurements in the intermediate region (X^* from 0.69 to 1.66) of a round jet of helium with their unheated air jet measurements and noted a marked increase in both the $u_{\rm rms}$ and $\overline{uv}$ measurements. Higher-order velocity correlations were larger than their air jet counterparts and the buoyant jet experienced a spreading rate larger than the homogeneous air jet. Triple correlations involving both concentration and velocity were measured and a kinetic energy and scalar budget were performed in the intermediate region. Data were also compared with predictions from Shih et al.'s (1987) model and the density fluctuations were concluded to have a passive effect on the structure of the flow, with the main effect coming from buoyancy forces.

Amielh et al. (1996) also took measurements in the intermediate region of a free jet of helium mixed with air and measured $u_{\rm rms}$ levels beyond an x/d of 30 similar to their free air jet levels. Their $u_{\rm rms}$ value is consistent with the helium-air jet work of So and Aksoy (1993) but is very much lower than Panchapakesan and Lumley's (1993) levels in the intermediate region. Amielh et al.'s (1996) measurements were taken in the near field of the jet (within x/d of 40), but their exit conditions meant that this region extended into the intermediate region of the jet, where buoyancy forces are not negligible.

Clearly, there is a lack of turbulence measurements spanning the intermediate region of a buoyant heated jet of air and the data that is available is inconsistent with other variable density jet data. However, indications are that a helium jet which results in density variations by mixing of two incompressible fluids leads to an increase in turbulence in the intermediate region while a heated jet for which density fluctuations are produced by heating, gives the opposite effect.

Turbulence models used for prediction of turbulent temperature fields require a link between the turbulent momentum and temperature fields. This is often provided through the dissipation time-scale ratio. Previous work in sodium, air and water jets has resulted in a relationship between the dissipation time-scale ratio and the fluid Prandtl number, Gehrke and Bremhorst (1993). The exact parameters affecting the time-scale ratio are not known but values ranging from 0.22 to 0.76 have been reported. Determination of the dissipation time-scale ratio for a strongly heated air jet will extend previous work and determine the influence of changing jet density.

Measurements of mean velocity and temperature data as well as second and third-order turbulence data to enable the dissipation time-scale ratio to be determined are presented. The data spans the inertia dominated and intermediate regions of a heated axisymmetric air jet issuing vertically into still air. The exit temperature was varied to allow the effect of different heating conditions to be determined.

2. Flow equations

The transport equations for turbulent kinetic energy, and mean square of the turbulent temperature fluctuations can be conveniently described for variable density flows by use of the Favre averaged turbulent kinetic energy and temperature variance. Favre weighted quantities are defined for the general variable y by Eq. (3)

$$y = \tilde{y} + y'', \tag{3}$$

where $\tilde{y}$ is the density weighted mean value given by $\overline{\rho y}/\bar{\rho}$ and y'' is the density weighted fluctuation of the variable given by $(y-\tilde{y})$ or $(y-\bar{y}-\overline{\rho' y'}/\bar{\rho})$. This decomposition can be applied to velocities, pressures, temperatures and kinetic energy, dissipation of turbulent kinetic energy as well as other flow variables and properties.

Application to a steady, axisymmetric jet without swirl and negligible viscous diffusion, leads to the turbulent kinetic energy transport equation, Eq. (4a), and temperature variance transport equation, Eq. (4b). The Favre weighted dissipation time-scale ratio is defined by Eq. (5)

$$\begin{aligned}
&\underbrace{\bar{\rho}\tilde{U}\frac{\partial k_{\rm f}}{\partial x} + \bar{\rho}\tilde{V}\frac{\partial k_{\rm f}}{\partial r}}_{\text{advection}} \\
&= \underbrace{\left[-\frac{1}{2}\frac{\partial}{\partial x}\left(\bar{\rho}\overline{u''u''u''} + \bar{\rho}\overline{u''v''v''} + \bar{\rho}\overline{u''w''w''} + 3\overline{pu''}\right)\right.}_{} \\
&\quad \underbrace{-\frac{1}{2}\frac{\partial}{\partial r}\left(\bar{\rho}\overline{v''u''u''} + \bar{\rho}\overline{v''v''v''} + \bar{\rho}\overline{v''w''w''} + 3\overline{pv''}\right)}_{} \\
&\quad \left.\underbrace{-\frac{1}{2}\left(\frac{\bar{\rho}\overline{u''u''v''}}{r} + \frac{\overline{\rho v''v''v''}}{r} + \frac{\bar{\rho}\overline{w''w''v''}}{r}\right)}_{\text{diffusion}}\right] \\
&\quad \left[+ \bar{\rho}\overline{u''u''}\frac{\partial \tilde{U}}{\partial x} + \bar{\rho}\overline{u''v''}\frac{\partial \tilde{U}}{\partial r} + \bar{\rho}\overline{v''u''}\frac{\partial \tilde{V}}{\partial x}\right. \\
&\quad \left. + \bar{\rho}\overline{v''v''}\frac{\partial \tilde{V}}{\partial r} + \bar{\rho}\overline{w''^2}\frac{\tilde{V}}{r}\right] \\
&\quad \underbrace{\qquad\qquad}_{\text{production}} \\
&\quad \underbrace{-\bar{u}''\frac{\partial \bar{P}}{\partial x}}_{\text{pressure}} \underbrace{-\frac{\overline{v''}}{r}\frac{\partial \bar{P}}{\partial r}}_{\text{work}} + \underbrace{\overline{p\frac{\partial u''}{\partial x}}}_{\text{pressure}} + \underbrace{\overline{\frac{p}{r}\frac{\partial (rv'')}{\partial r}}}_{\text{dilation}} - \underbrace{\bar{\rho}\varepsilon_{k_{\rm f}}}_{\text{dissipation}},
\end{aligned} \tag{4a}$$

$$\underbrace{\bar{\rho}\tilde{U}\frac{\partial\overline{t''^2}}{\partial x}+\bar{\rho}\tilde{V}\frac{\partial\overline{t''^2}}{\partial r}}_{\text{advection}} = \left[\underbrace{-\frac{\partial}{\partial x}\left(\bar{\rho}\overline{u''t''^2}\right)-\frac{\partial}{\partial r}\left(\bar{\rho}\overline{v''t''^2}\right)-\frac{\bar{\rho}\overline{v''t''^2}}{r}}_{\text{diffusion}}\right] - \left[\underbrace{2\bar{\rho}\overline{u''t''}\frac{\partial\tilde{T}}{\partial x}-2\bar{\rho}\overline{v''t''}\frac{\partial\tilde{T}}{\partial r}}_{\text{production}}\right] - \underbrace{2\bar{\rho}\varepsilon_{\overline{t''^2}}}_{\text{dissipation}}, \quad (4b)$$

$$R=\left(\frac{\varepsilon_{k_f}}{2k_f}\frac{\overline{t''^2}}{\varepsilon_{\overline{t''^2}}}\right). \quad (5)$$

The above equations form the basis for subsequent data reduction. Density fluctuations were obtained through the perfect gas equation with the assumption of constant pressure. This is justified on the basis that density fluctuations resulting from temperature changes are much larger than those due to mechanical processes associated with inertia and shear effects, as only flow at low, subsonic Mach numbers will be considered here. Consequently, the relationship $\rho=\bar{P}_{amb}/RT$ was used.

3. Experimental apparatus and techniques

The jet was produced by a nozzle with a cubic contour, Hussain and Ramjee (1976), with an exit diameter of 10 mm, upstream diameter of 67 mm and length of nozzle of 67 mm. Air was sourced from a wind tunnel outlet in order to give the required constancy of mass flow. The nozzle was preceded by a settling section containing heater elements and a mixing and a smoothing section designed to give uniform temperature of air flow across the exit plane. The nozzle and its settling section were located vertically so that the gravity vector opposed the airflow.

Simultaneous velocity and temperature measurements were taken with a Dantec triple wire probe. Two inclined Wollaston wires of 5 μm diameter and approximate length of 1.2 mm for the exposed length, formed an *X*-array to measure velocity in the streamwise and radial directions. A nearby temperature wire of 2.5 μm diameter and 1 mm exposed length spanning the full distance between the supporting prongs, measured flow temperature. Lateral separation of the wires was approximately 1 mm. The temperature wire was inclined to be parallel to the nearest velocity wire. This was found to reduce thermal contamination from the velocity wire and also reduced the array spatial dimensions thus improving the spatial resolution. The *X*-array wires were operated with a Disa 55M01/11 CTA bridge while the temperature wire was operated with a modified Disa 55M01/20 constant current unit. The modifications are

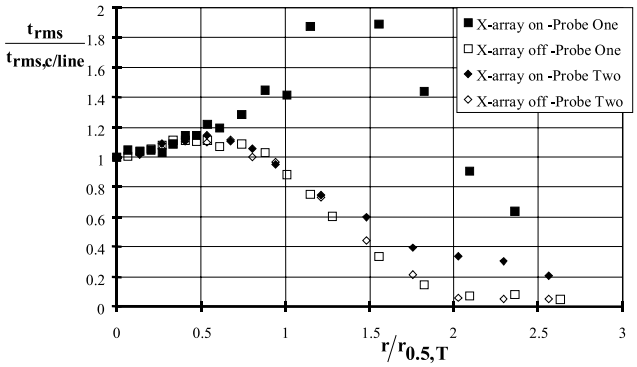

Fig. 1. Comparison of t_{rms} measured with the temperature wire of probe 1 and probe 2 at $x/d=60$, exit temperature = 110 °C above ambient.

fully described by Bremhorst and Krebs (1976) and are designed to give full cable compensation so that correct wire corner frequency measurements could be carried out. Calibration of the inclined wires was similar to the method described by Bremhorst and Gehrke (2000) while temperature compensation followed the methods described by Graham and Bremhorst (1990).

The original probe (referred to as probe 1) had the temperature wire normal to the mean flow, to one side of the *X*-array and located near the centre of the *X*. Fig. 1 shows the significant thermal contamination produced by the geometry of probe 1 in the outer region of the jet. Placing the temperature wire upstream of the centre of the *X* is known to reduce thermal contamination from the inclined wires to the temperature wire, Antonia et al. (1980), but this reduces spatial resolution. Using an inclined temperature wire parallel to the nearest inclined *X*-wire (probe 2), is seen to virtually eliminate thermal contamination, Fig. 1, while reducing wire separation. Results presented in Section 4 were taken with probe 2.

A second effect is one of heat conduction from the hot inclined wires to the temperature wire at very low velocities. This is due to the temperature boundary layer which forms around the hot inclined wires and exists

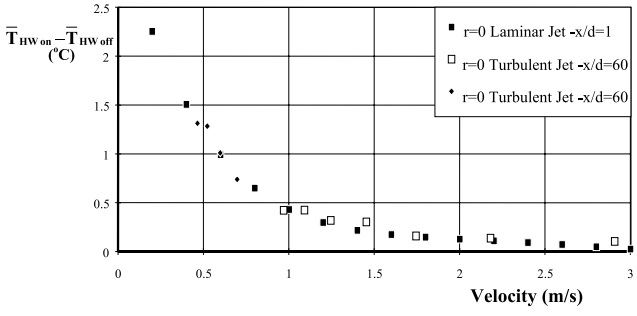

Fig. 2. Difference in temperature wire output with and without current through velocity wires (probe 2) for a very low turbulence (laminar) jet and two different turbulent jets operated at various exit velocities.

even in the upstream direction. Fig. 2 illustrates the significance of the effect in a very low turbulence flow (laminar case in Fig. 2) as well as in the turbulent core of the jet. It is seen to become increasingly significant below 2.5 m/s. A correction was introduced to the mean temperature of the temperature wire during data reduction. Tests, Anderson (2000), showed this to lead to a significant improvement of measured mean and fluctuating quantities.

Jet exit conditions were measured to test symmetry and turbulence levels. Mean velocity and mean temperature profiles were flat (top hat) with little evidence of nozzle boundary layer formation. While turbulence levels were below 1%, temperature fluctuation levels were up to 2% relative to the exit temperature excess, $\Delta\bar{T}_{ex}$, and were uniform across the jet up to jet exit temperatures of 350 °C which is the limit for structural integrity of the probe.

4. Results

4.1. Centreline decay of mean velocity and mean density

The present jet operating data is summarised in Table 1. The decay of centreline mean axial velocity is presented in Fig. 3 in terms of dimensionless variables, U^* and X^* where the former is defined by Eq. (6a). Excess density is defined by Eq. (6b) and is shown in Fig. 4

$$U^* = Fr^{1/2}\left(\frac{\bar{\rho}_{ex}}{\rho_{amb}}\right)^{-1/4}\frac{\bar{U}_{c/line}}{\bar{U}_{ex}}, \tag{6a}$$

$$g^* = Fr^{1/2}\left(\frac{\bar{\rho}_{ex}}{\rho_{amb}}\right)^{3/4}\frac{\rho_{amb}-\bar{\rho}_{c/line}}{\rho_{amb}-\bar{\rho}_{ex}}. \tag{6b}$$

The present data collapses well onto the curves recommended by Chen and Rodi (1980) for the inertia dominated region but deviates slightly in the intermediate region of the heated jet.

4.2. Centreline decay of turbulent quantities

Turbulence velocities, u_{rms} and v_{rms}, Fig. 5, were lower in the intermediate region of the jet than in the

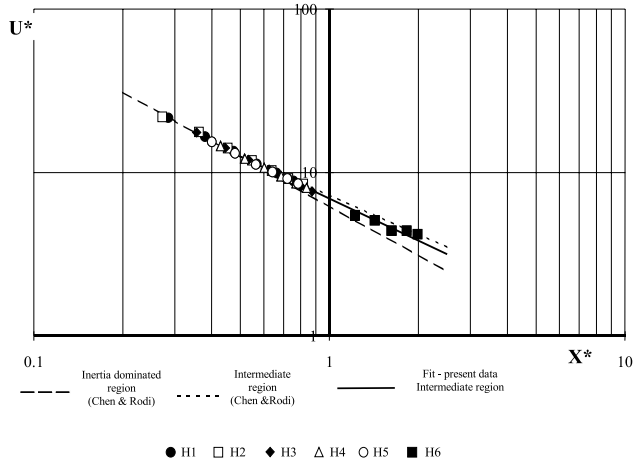

Fig. 3. Decay of normalised centreline velocity (U^*) in heated jet.

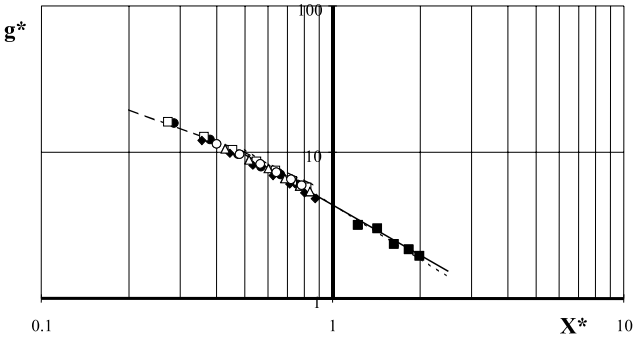

Fig. 4. Decay of normalised centreline excess density (g^*) for meaning of symbols and lines refer to Fig. 3.

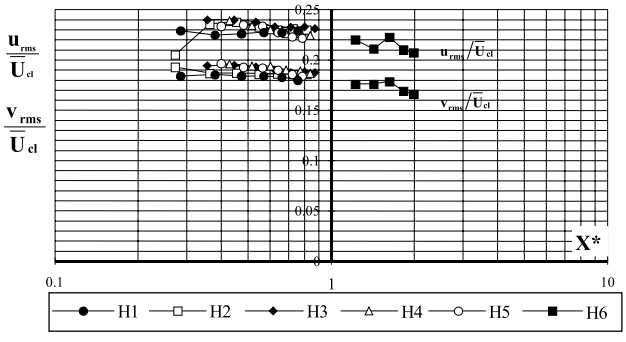

Fig. 5. Decay of centreline turbulence intensity.

Table 1
Experimental conditions for heated jets investigated

	$\bar{U}_{ex}$ (m/s)	$\Delta\bar{T}_{ex}$ (°C)	Reynolds no.	Froude no.	$\bar{\rho}_{ex}/\rho_{amb}$	X^* range
H1	22.4	118	7880	13,190	0.7209	0.3–0.8
H2	35.8	240	8500	16,021	0.5508	0.27–0.81
H3	44.4	332	7900	18,300	0.4853	0.38–0.92
H4	54.3	430	7700	21,100	0.4123	0.45–0.9
H5	65.4	520	7560	25,600	0.3698	0.39–0.78
H6	19.15	322	3470	3500	0.4849	1.22–1.98

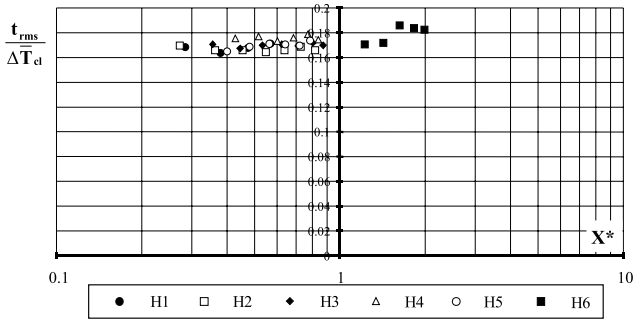

Fig. 6. Decay of t_{rms} at centreline of jet.

inertia dominated region. These levels are also lower than those measured in the unheated jet. Peterson and Bayazitoglu's (1992) measurements in a heated air jet also indicated a decrease in turbulence levels in this region when compared with their unheated jet. Panchapakesan and Lumley's (1992) measurements in the intermediate region of a helium jet on the other hand were noted to be almost twice as large as in the inertia dominated region of their air jet. A gradual increase in t_{rms} at the jet centreline with increasing X^* is noted in the present measurements, Fig. 6.

4.3. Radial distributions of mean and turbulence quantities

Full radial profiles of the Reynolds averaged mean and turbulent quantities were taken for the various heating levels. While profiles for all six heating cases are available, Anderson (2000), only the two extreme cases, H2 and H6, are presented here for brevity – the former being predominantly in the inertia dominated region while the latter is entirely in the transition region. These are included in Appendix A and are given in full for the H6 case but with a line of best fit to the H2 data added for ease of comparison. Reynolds averaged variables are presented in order to be consistent with published data. Curves shown were fitted to the data using the equations listed in Appendix B. The curve of best fit for unheated velocity data obtained with the same apparatus and measurement techniques, is included for comparison. Mean velocity and temperature data is also compared with the Gaussian profile.

A common feature of the radial distributions, Figs. 15–30, is apparent self-similarity in the sense that no x/d dependence was discernible. However, there were some noticeable changes to the data taken well within the intermediate region, H6, when compared with data taken in the end of the inertia region and to the beginning of the intermediate region, H1–H5. Mean streamwise velocity distributions, Fig. 15, showed a strong effect in the tails of the distributions beyond the half centreline value. $\bar{V}, \Delta\bar{T}$, and t_{rms} showed no discernible effects in the intermediate region, but $u_{rms}, \overline{uv}, \overline{u^3}, \overline{u^2v}$ and $\overline{uv^2}$ are seen to lose symmetry for the H6 case located in the intermediate region. The asymmetry is seen as a difference in peak value for negative r. Cross-products involving fluctuating temperature, $\overline{ut^2}, \overline{vt^2}$, and $\overline{t^3}$ are not symmetrical for all heating cases considered. Furthermore, $\overline{vt^2}$ is offset in the negative direction. The reason for these deviations from symmetry is given in Section 4.6.

4.4. Energy and temperature variance budgets

Figs. 7(a) and (b) and 8(a) and (b) show the kinetic energy and temperature variance budgets for heated cases H2 and H6. Favre averaged quantities were obtained to give estimates of the turbulent kinetic energy and temperature variance budgets from Eqs. (4a) and (4b). Normalisation of the various terms of Eqs. (4a) and (4b) is with $(r_{0.5,\tilde{U}})/(\bar{\rho}\tilde{U}^3)_{c/line}$ and $(r_{0.5,\tilde{U}})/(\bar{\rho}\tilde{U}\Delta\tilde{T}^2)_{c/line}$, respectively. Due to the rapid drop of temperature from the jet exit, temperature induced density fluctuations were very small. Consequently, even at the highest heating rate, $\bar{U} = \tilde{U}$ and $\bar{T} = \tilde{T}$ within 2% at the downstream positions reported here. The dissipation term (Diss.) was calculated as the sum of the advection (Adv.), diffusion (Diff.), production (Prod.) and buoyancy (pressure work term in the kinetic energy budget only, Buoy.) terms. Pressure components were not measured, and hence the dissipation term is actually the summation of dissipation and pressure terms which include pressure diffusion and pressure dilation. This is similar to the approach taken by Panchapakesan and Lumley (1993) and Dai et al. (1995). Budget terms were calculated from least squares curve fits to each x/d profile. As the azimuthal velocity was not measured in the present experiments, the diffusion term $\overline{v''w''^2}$ was taken equal to $\overline{v''^3}$ and the production term, $\overline{w''^2}\overline{V}/r$ taken to be equal to $\overline{v''^2}\overline{V}/r$, consistent with Panchapakesan and Lumley (1993).

In cases where radial distributions displayed some offset and asymmetry, only the positive radial part of the distribution was used for subsequent determination of budgets. Although the diffusive term involving $\overline{u_i''u_j''u_j''}$ is a minor one, a decomposition shows that of its six non-zero components, the one most affected by errors is $\overline{v''^3}/r$. The limit of this term tends towards $\mathrm{d}\overline{v''^3}/\mathrm{d}r$ as $r \to 0$ and can only be satisfied by removal of the offset. Without removal of the offset, a large anomalous value is obtained for $\overline{v''^3}/r$. Removal of the offset does not alter the $\mathrm{d}\overline{v''^3}/\mathrm{d}r$ term. Similar considerations apply to $\overline{v''t''^2}$ profiles.

The overall shapes of the kinetic energy budgets follow trends similar to those of unheated data obtained in the present jet and data of others. Comparison of H1–H5 data not shown here, which spans the end of the inertia region ($X^* = 0.3$–0.9) shows an X^* dependency for advection which decreases with increasing X^*.

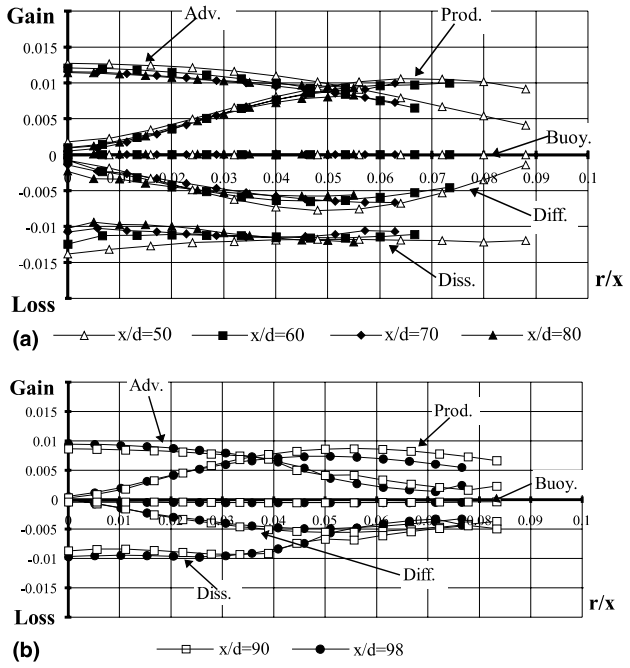

Fig. 7. (a) Kinetic energy budget for heated case H2; (b) kinetic energy budget for heated case H6.

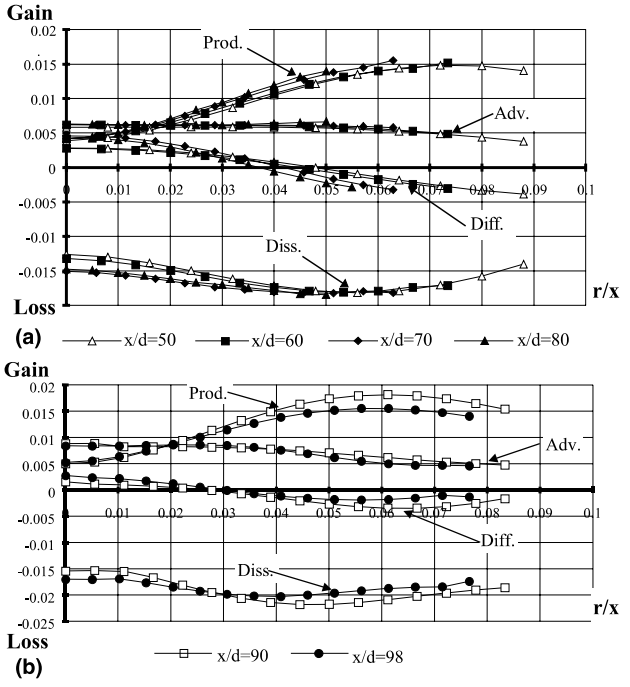

Fig. 8. (a) Temperature variance budget for heated case H2; (b) temperature variance budget for heated case H6.

Comparison of Fig. 7(a) and (b) further illustrates that increased X^* decreases advection and production of turbulent kinetic energy. This may explain the decrease

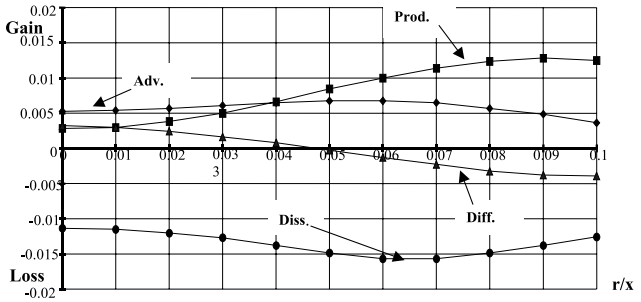

Fig. 9. Scalar variance budget reproduced from Panchapakesan and Lumley (1993).

of u_{rms} in the intermediate region. Panchapakesan and Lumley's (1993) results show much higher levels of turbulent kinetic energy production and advection in the helium jet for which u_{rms} was noted to be higher in the intermediate region.

Overall, the temperature variance budgets for each x/d collapse well and the combined profiles have little scatter. Advection levels in the core are higher in the intermediate region. No dependency of advection on heating level or X^* was noticed for the H1–H5 cases. Peak production levels, however, increase with increasing heating levels while diffusion decreases with increasing levels of heating. The peak production for H2 is +0.015, while for the H5 case, not shown here, it is +0.018. Peak production levels for H6 range between +0.015 and +0.017. Levels are higher than Panchapakesan and Lumley's (1993) helium jet, Fig. 9, which show a peak production of +0.013. Also, production values of 0.004 at the jet centreline are slightly higher than Panchapakesan and Lumley's (1993) value of +0.003. Panchapakesan and Lumley's (1993) results are not for a specific x/d position as the data was based on fits to self-similar profiles. Peaks are at a similar radial location to present measurements.

4.5. Dissipation time-scale ratio results

The dissipation time-scale ratio was calculated from radial profiles of kinetic energy and scalar variance budgets. The resulting radial profiles of dissipation time-scale are presented in Figs. 10(a) and (b) which show a definite, consistent trend with axial location. At lower x/d levels for the H2 case, the ratio varies between 0.35 and 0.5 across the radial range considered while at higher x/d levels, the ratio is relatively constant with a value between 0.3 and 0.35. The levels for the H6 case vary between 0.3 and 0.35 over the range considered. Comparison of data at all heating levels shows that there is no obvious trend dependent on heating levels in the inertia dominated region and data are not affected by

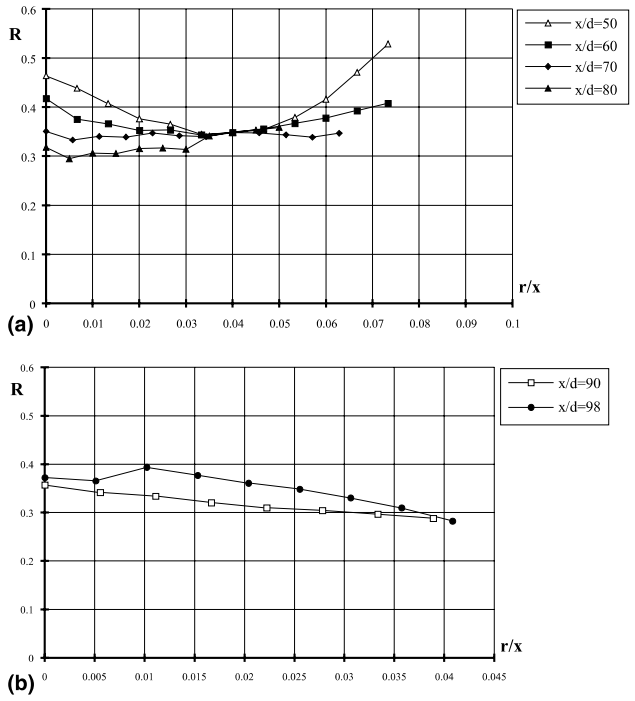

Fig. 10. (a) Dissipation time-scale ratio for case H2 based on budgets of Figs. 7(a) and 8(a); (b) dissipation time-scale ratio for case H6 based on budgets of Figs. 7(b) and 8(b).

buoyancy forces as seen from data at the higher X^* values in the transition region.

Time-scale ratio levels are, however, lower than reported by others. Gehrke and Bremhorst (1993) reported values for a multi-bore jet block flow where one jet was slightly heated. The resulting flow was like a grid flow and the results predict a dissipation time-scale ratio for the present experimental conditions to be 0.633. Panchapakesan and Lumley (1993) measured a ratio of between 0.58 and 0.69 in the intermediate region of the helium jet. Their results were based on self-similar experimental profiles removing the possibility of identifying any axial trends which deviate from scaling inherent in assuming self-similarity. Dai et al. (1995) calculated dissipation time-scale ratio values ranging between 0.22 and 0.51 in the self-preserving region of a turbulent buoyant plume of CO_2.

The accepted value of time-scale ratio used for modelling is 0.5. Gharbi et al. (1996) used a time-scale ratio of 0.5 and found good agreement between experimental profiles using Panchapakesan and Lumley's (1993) helium jet data and their model. Sanders et al. (1996) using first- and second-order models calculated a range of time-scale ratio centreline values between 0.4 and 0.76 with some models predicting variations of the order of 0.5 over the width of the jet. These variations could be due to differences in modelling the dissipation term with Ruffin et al. (1994) calculating a time-scale ratio of 0.38 for the centreline of a round circular heated jet of air. The study also concluded that the time-scale ratio did not depend on density ratio or Reynolds number.

4.6. Possible reasons for lower time-scale ratio values

The low values of dissipation time-scale ratio obtained from present experimental data can be due to variations in the flow quantities $k_f, \varepsilon_{k_f}, \overline{t''^2}$ and $\varepsilon_{\overline{t''^2}}$. In particular, the levels of temperature intensity for present measurements are lower than reported by others (by about 0.04), which would result in lower levels of dissipation time-scale ratio by approximately 0.2. Levels of dissipation of temperature variance are high when compared with Panchapakesan and Lumley's (1993) helium jet which would also result in a lower calculated value of dissipation time-scale ratio.

Profiles of $\overline{ut^2}$ and $\overline{vt^2}$ shown in Appendix A, were noticeably non-symmetrical about the jet centreline and $\overline{vt^2}$ had a negative offset. Other mean and turbulent data indicated the jet was symmetric. Further investigations reported more fully by Bremhorst and Anderson (2001) suggest the leading prong of the inclined wire alters the temperature flow field around it and hence around the temperature wire. Using the flow angle defined relative to the probe as shown in Fig. 11, temperature data at radial positions either side of the jet centreline is compared in Fig. 12(a) on the basis of flow from a particular flow angle. The ordinate in this figure is the average temperature for each flow angle less the total local mean temperature. Results for one radial position are rotated about the jet axis allowing comparison of the same flow on opposite sides of the jet. It can be seen that above an angle of 12°, the distributions of temperature differ markedly. Similar data for a temperature wire normal to the bulk flow (probe 1) revealed coincident distributions, Fig. 12(b).

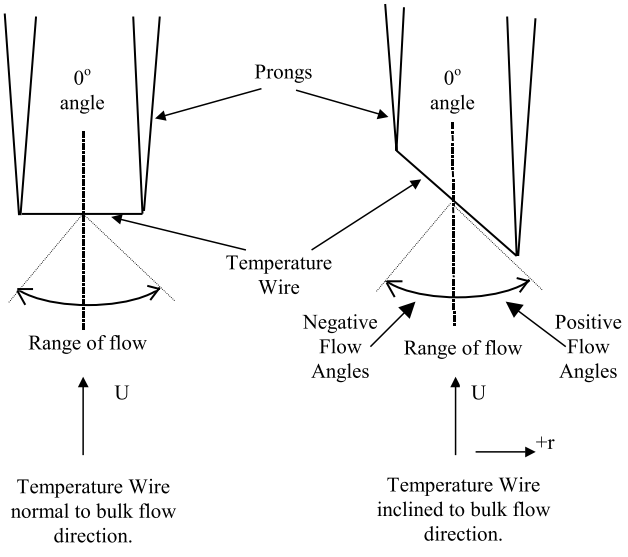

Fig. 11. Schematic of flow over normal and inclined wire.

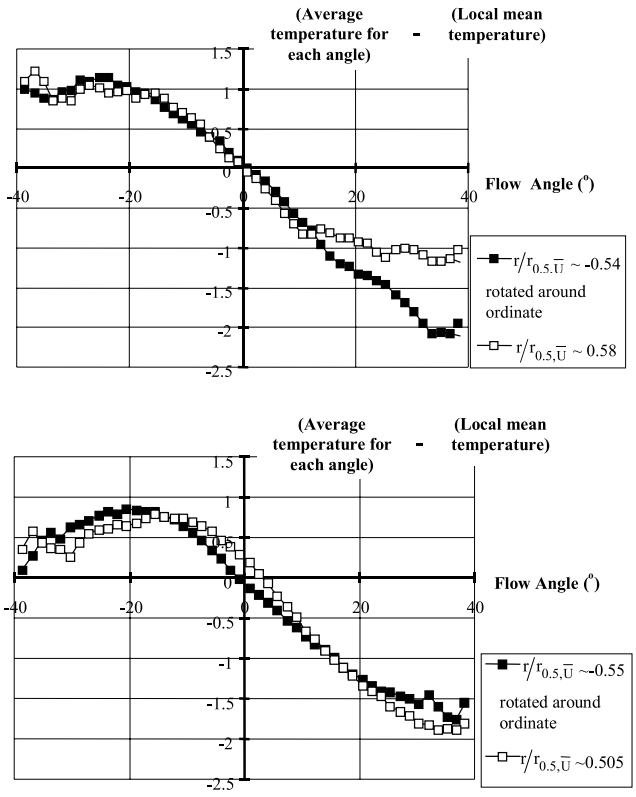

Fig. 12. (a) Average temperature for each angle for inclined temperature wire at $r/r_{0.5,\bar{U}}$ of +0.58 and −0.54; (b) Average temperature for each angle for normal temperature wire at $r/r_{0.5,\bar{U}}$ of +0.505 and −0.55.

The attenuation of temperature noted in Fig. 12(a) when the flow is at high positive flow angles, can be explained in terms of an effect of a thermal wake from the leading prong. Both temperature wire prongs have a large thermal inertia and in the turbulent flow would be at the mean temperature. Flow with temperature fluctuations below the mean temperature would result in a thermal wake with a relatively higher air temperature and stream temperatures above the mean temperature would produce a thermal wake with a relatively lower air temperature at large positive flow angles. Thus, the flow at these angles either gains or loses heat, depending on the relative difference between the flow temperature and prong temperature. Since the wake crosses the temperature wire, the temperature wire measures a distorted temperature value. When the raw data were analyzed without large flow angles, that is, excluding data when flow is almost parallel to temperature wire, $\overline{t^3}$ profiles were observed to be more symmetric and in the case of $\overline{vt^2}$, centred around zero. The effect of the inclined temperature wire is also seen to underestimate the dissipation time-scale ratio. This as yet unreported but complex phenomenon could potentially also affect measurements taken with inclined velocity wires. Due to the symmetry of conventional multi-wire arrays, the effect may have gone unnoticed.

5. Eddy diffusivity and scalar variance model constants

From the data obtained, various modelling approaches can be examined. The isotropic eddy diffusivity model for the steady, axisymmetric jet without swirl is given by Eq. (7a) which can be written in the form of Eq. (7b) by use of the eddy diffusivity, Eq. (7c), and the turbulent Prandtl number, σ_t. Taking typical model values of $C_\mu = 0.09$ and $\sigma_t = 0.6$, means $C_\mu/\sigma_t = 0.15$

$$\overline{v''t''} = -v_\theta \frac{\partial \tilde{T}}{\partial r}, \tag{7a}$$

$$\overline{v''t''} = -\frac{C_\mu}{\sigma_t}\frac{k_f^2}{\varepsilon_{k_f}}\frac{\partial \tilde{T}}{\partial r}, \tag{7b}$$

$$v_t = C_\mu \frac{k_f^2}{\varepsilon_{k_f}}. \tag{7c}$$

The generalised gradient hypothesis, Eq. (8a), where the constant C_θ takes the value 0.3, reduces to Eq. (8b) for the steady, axisymmetric jet free of swirl.

$$\overline{u_i''t''} = -C_\theta \frac{k_f}{\varepsilon_{k_f}}\overline{u_i''u_j''}\frac{\partial \tilde{T}}{\partial x_j}, \tag{8a}$$

$$\overline{v''t''} = -C_\theta \frac{k_f}{\varepsilon_{k_f}}\left[\overline{u''v''}\frac{\partial \tilde{T}}{\partial x} + \overline{v''^2}\frac{\partial \tilde{T}}{\partial r}\right]. \tag{8b}$$

The generalised equation for scalar variance, Eq. (9a) simplifies to Eq. (9b) for the present jet. The coefficient C_t can be obtained from Eqs. (4b) and (5) by neglecting advection and diffusion to give a value of 1.0 if the time-scale ratio is assumed to be 0.5.

$$\overline{t''^2} = -C_t \frac{k_f}{\varepsilon_{k_f}}\overline{u_i''t''}\frac{\partial \tilde{T}}{\partial x_i}, \tag{9a}$$

$$\overline{t''^2} = -C_t \frac{k_f}{\varepsilon_{k_f}}\left[\overline{u''t''}\frac{\partial \tilde{T}}{\partial x} + \overline{v''t''}\frac{\partial \tilde{T}}{\partial r}\right]. \tag{9b}$$

Correlation coefficients relating fluctuating velocity and temperature, Eq. (10), are useful for interpretation of flow structure as well as for comparison with other similar flows.

$$R_{u_i''t''} = \frac{\overline{u_i''t''}}{\sqrt{\overline{u''^2}\,\overline{t''^2}}}. \tag{10}$$

Figs. 13(a) and (c) show the distributions of the above constants in the momentum part of the jet based on the H2 Favre averaged data using curves of best fit, while Figs. 14(a) and (b) give the two non-zero correlation coefficients. In the case of the isotropic eddy diffusivity

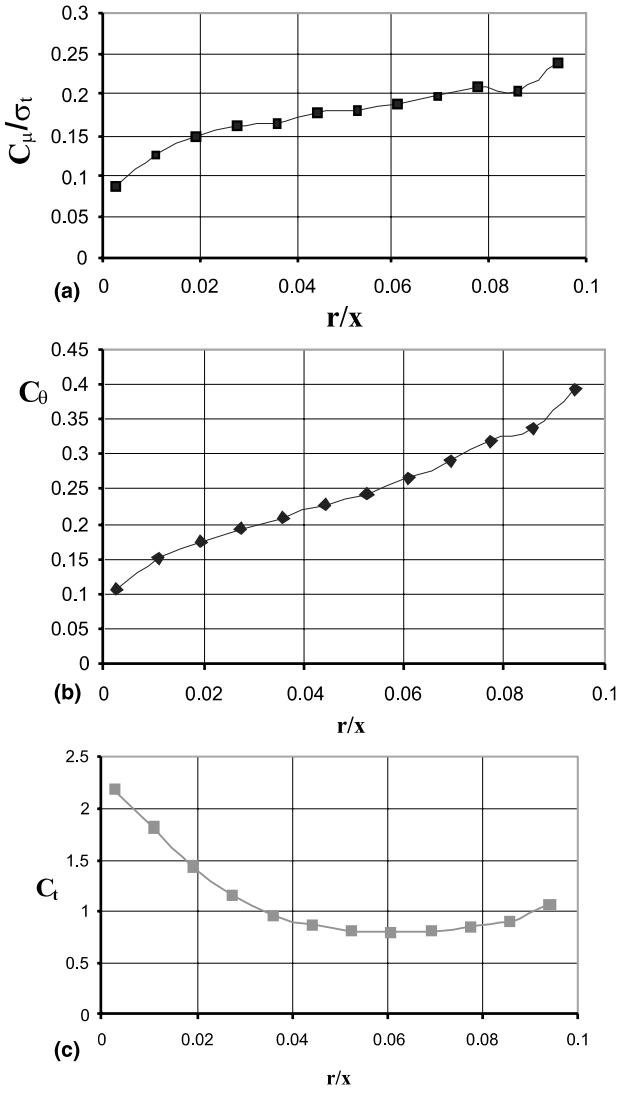

Fig. 13. (a) Isotropic eddy diffusivity model constant, $x/d = 60$, estimated error = ±16%; (b) generalised eddy diffusivity model constant, $x/d = 60$, estimated error = ±20%; (c) scalar variance model constant, $x/d = 60$, estimated error = ±20%.

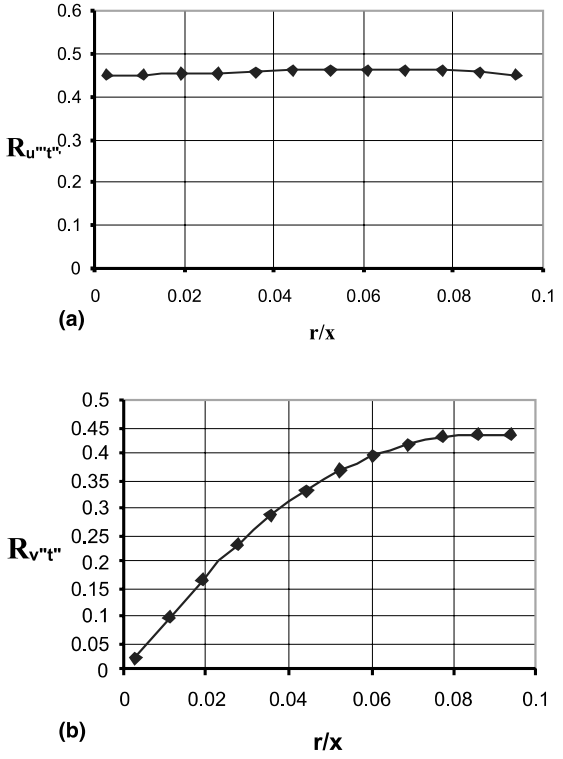

Fig. 14. (a) Correlation coefficient of streamwise velocity fluctuation and temperature fluctuation, $x/d = 60$, estimated error = ±9%; (b) correlation coefficient of radial velocity fluctuation and temperature fluctuation, $x/d = 60$, estimated error = ±9%.

model, measured data is in the range $0.076 < C_\mu/\sigma_t < 0.24$ which spans the model value of 0.15. C_θ varies considerably across the flow but is centred around the generally accepted model constant of 0.3. The scalar variance model constant, $C_t = 1.0$, shows good agreement with measured values in the shear dominated region of the flow but does deviate noticeably in the central region where advection and diffusion become significant. The correlation coefficients are consistent with those found, for example, in fully developed pipe and boundary layer flows. In both cases the streamwise velocity fluctuations correlate well with the temperature fluctuations. The correlation of radial velocity fluctuation and temperature fluctuation must vanish at the centreline but increase to a range of 0.4–0.5 in the fully developed shear region where production and dissipation of turbulent fluctuations reach a balance.

An error analysis based on 95% confidence limits was carried out for all directly measured variables. From these and the use of simplifying assumptions relating to dissipation rates, errors were evaluated for the various diffusivity model constants and are indicated in figure captions. Uncertainties associated with the simplifying assumptions relating to azimuthal turbulence components and pressure terms are not included in these estimates.

Turbulent Prandtl numbers calculated with Eq. (11) using the present experimental data, range from 0.97 at $r/x = 0.01$ to 1.09 at $r/x = 0.1$. This may appear to contradict the model value of 0.6 used for the isotropic eddy diffusivity model of above, however, as one model is based on Eq. (11) and the other on turbulent kinetic energy and dissipation rate, Eq. (7b), such a difference is not surprising. If the above values are used for modelling of eddy diffusivity of heat, satisfactory values will be obtained with either model provided that model constants and definitions are not mixed. Since Reynolds and Favre averages were within 1–2% of each other, turbulent Prandtl number is unaffected by density weighting, at least within experimental accuracy.

$$\sigma_t = \frac{\overline{u''v''}}{\partial\tilde{U}/\partial r}\,\frac{\partial\tilde{T}/\partial r}{\overline{v''t''}}. \tag{11}$$

6. Conclusions

Mean centreline velocity and temperature data were affected by increasing influence of buoyancy in the intermediate region of the heated jet. The decay of these quantities was consistent with the decay laws of Chen and Rodi (1980). Normalised levels of $u_{\rm rms}$ and $v_{\rm rms}$ showed a decrease in the intermediate region of the heated jet relative to the inertia dominated region as well as the unheated case and is contrary to the case of a helium jet for which turbulence levels in the intermediate region are about twice those in the inertia dominated region. In the core of the flow, increased heating was found to decrease advection and production of turbulent kinetic energy but increases advection of temperature variance. An increase of heating also lowers the contribution of diffusion of temperature variance.

The dissipation time-scale ratio was found to be unaffected for the range of heating levels considered. A definite trend of the radial distributions with x/d locations was found with the ratio becoming constant across the jet at larger x/d.

Investigations into the asymmetries observed in triple correlation profiles, $\overline{ut^2}$, $\overline{vt^2}$, and $\overline{t^3}$ highlighted a problem with using an inclined temperature wire in a turbulent heated flow field even though temperature is a scalar for which the orientation of the cold wire, which is sensitive only to temperature, should not matter. The resultant error was found to be responsible for the asymmetries found in the higher order correlations and for the lower measured values of dissipation time-scale ratio. The full effect of this newly defined phenomenon is still to be explored and may extend to the temperature component of inclined velocity wires which are usually velocity and temperature sensitive in highly heated flows.

Constants often used for the isotropic, the generalised gradient hypothesis and the scalar transport models were obtained from the data. These are within the range normally used but the generalised gradient hypothesis constant shows considerable variation across the flow. Correlation coefficients relating fluctuating velocity and fluctuating temperature are similar to those found in fully developed boundary layer and pipe flows. Turbulent Prandtl numbers are in the range of 0.97–1.09.

Appendix A. Radial distributions of heated jet flow variables

See Figs. 15–30.

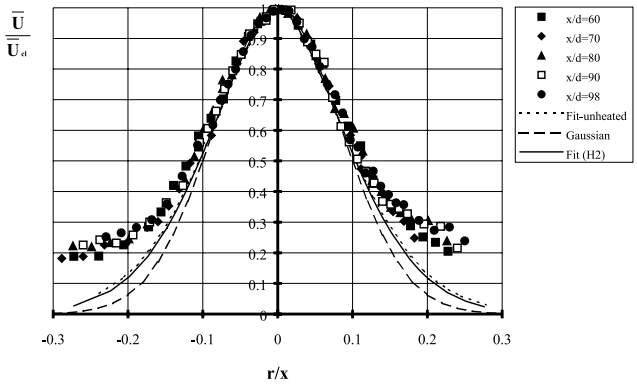

Fig. 15. $\bar{U}$ normalised radial profile, H6 case. H2 data fit using Eq. (B.1) with coefficients $a = -34.478$, $b = 1.7282$.

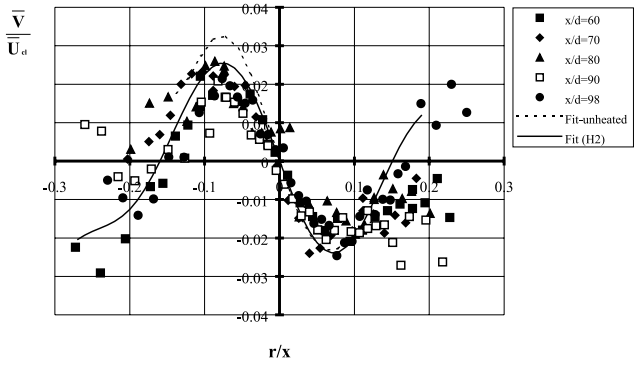

Fig. 16. $\bar{V}$ normalised radial profile, H6 case. H2 data fit using 6th-order polynomial, Eq. (B.8) with coefficients $a_1 = -1.754e3$, $a_2 = -1.023e2$, $a_3 = 4.0181e1$, $a_4 = 4.7035e1$, $a_5 = -6.3134e-2$, $a_6 = -5.6882e-2$, $a_7 = 2.7277e-4$.

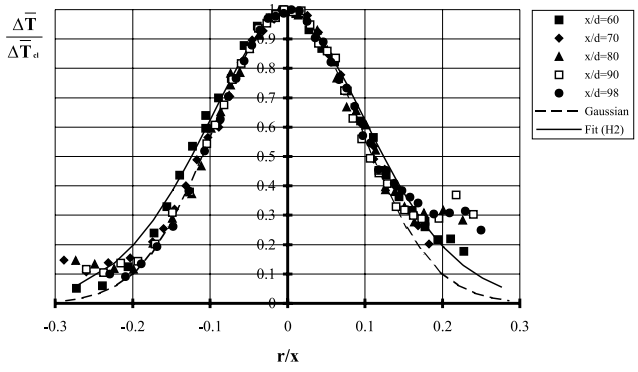

Fig. 17. $\Delta\bar{T}$ Normalised profile, H6 case. H2 data fit using Eq. (B.1) with coefficients $a = -28.9205$, $b = 1.7871$.

Appendix B. Curve fit equations

The following equations developed by Gehrke (1997) were used when fitting data for the unheated and heated jet experiments. Since the $\overline{v^3}$ profiles were not centred

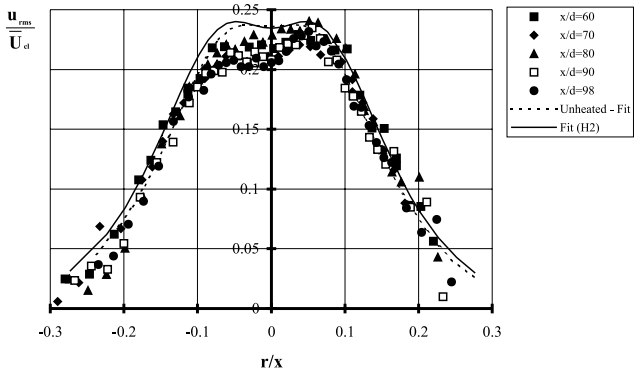

Fig. 18. u_{rms} normalised profiles, H6 case. H2 data fit using Eq. (B.2) with coefficients $a = 5.6319$, $b = -152.9937$, $c = -53.975$.

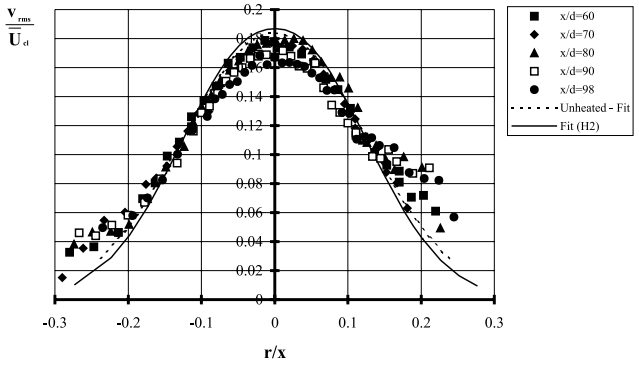

Fig. 19. v_{rms} normalised profiles, H6 case. H2 data fit using Eq. (B.3) with coefficients $a = 0.0349$, $b = -99.9935$, $c = 2.1931$.

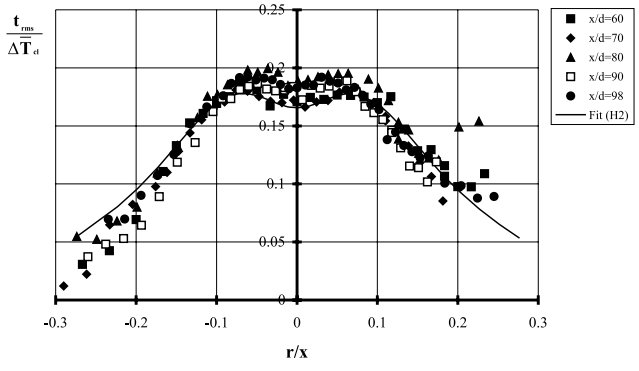

Fig. 20. t_{rms} normalised profiles, H6 case. H2 data fit using Eq. (B.2) with coefficients $a = 3.1155$, $b = -132.76$, $c = 0.0274$, $d = -29.6543$.

around zero at the jet centreline, it was found that using a modelled equation which would be forced through zero at the jet centreline (as the $\overline{v^3}$ should), would result in a radial gradient far greater than in reality. To achieve greater accuracy for this gradient, an nth-order polynomial was fitted to the $\overline{v^3}$ data. $\bar{V}$, $\overline{ut^2}$ and $\overline{vt^2}$ data were also fitted with the nth-order polynomial.

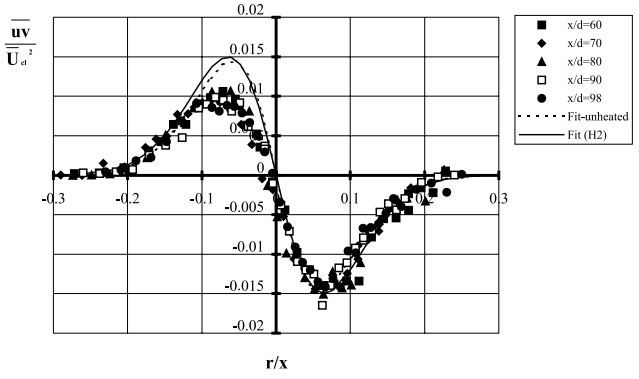

Fig. 21. $\overline{uv}$ normalised profile, H6 case. H2 data fit using Eq. (B.4) with coefficients $a = 0.41$, $b = -70.382$, $c = 1.758$.

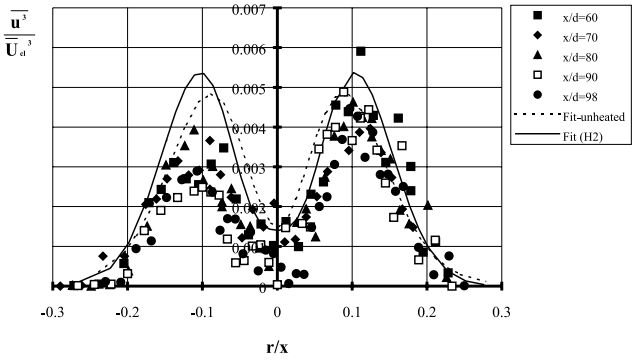

Fig. 22. $\overline{u^3}$ normalised profiles, H6 case. H2 data fit using Eq. (B.5) with coefficients $a = 1.2676$, $b = -129.83$, $c = 2.179$, $d = 0.0014$, $e = -736.16$.

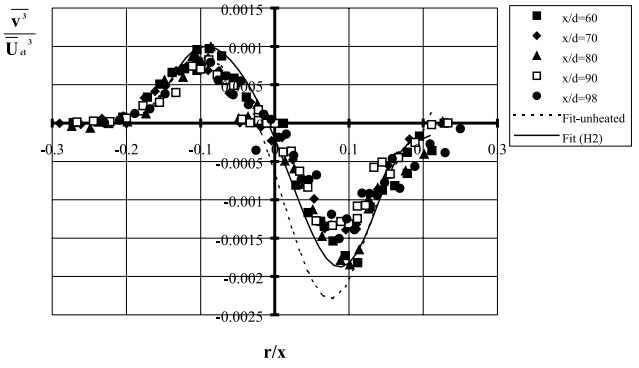

Fig. 23. $\overline{v^3}$ normalised profiles, H6 case. H2 data fit using 10th-order polynomial, Eq. (B.8) with coefficients $a_1 = -5.97\mathrm{e}4$, $a_2 = 1.9891\mathrm{e}4$, $a_3 = 8.0687\mathrm{e}3$, $a_4 = -1.859\mathrm{e}3$, $a_5 = -4.1237\mathrm{e}2$, $a_6 = 3.9043\mathrm{e}1$, $a_7 = 9.6166$, $a_8 = 6.9755\mathrm{e}-1$, $a_9 = -8.3402\mathrm{e}-2$, $a_{10} = -2.3297\mathrm{e}-2$, $a_{11} = -2.0614\mathrm{e}-4$.

$$\frac{\bar{U}}{\bar{U}_{\mathrm{c/line}}} = \mathrm{e}^{a(r/x)^b}, \text{ also used for mean temperature,} \tag{B.1}$$

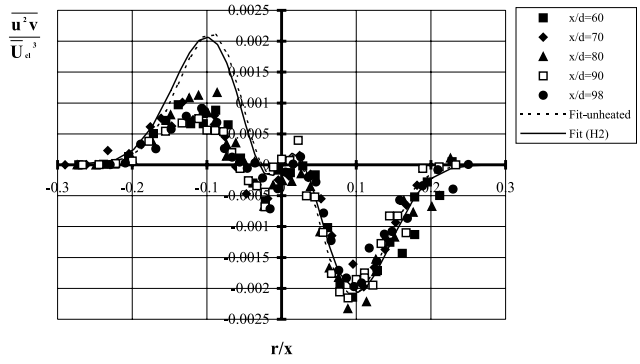

Fig. 24. $\overline{u^2v}$ normalised profiles, H6 case. H2 data fit using Eq. (B.6) with coefficients $a = 0.497$, $b = -200.0017$, $c = 2.3619$, $d = -0.0225$, $e = -500.0014$.

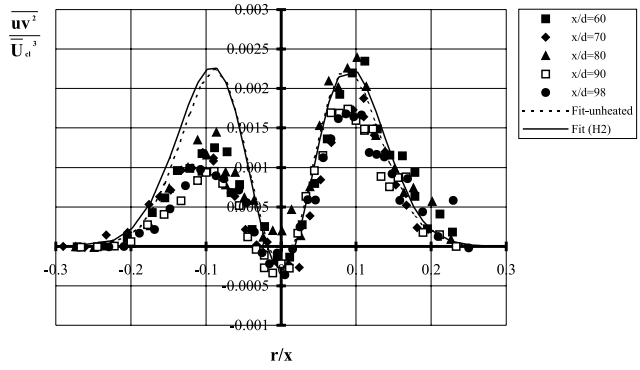

Fig. 25. $\overline{uv^2}$ normalised profiles, H6 case. H2 data fit using Eq. (B.7) with coefficients $a = 0.8787$, $b = -107.4634$, $c = 1.9322$, $d = -0.0003$, $e = -550.3388$, $f = 3.7469$.

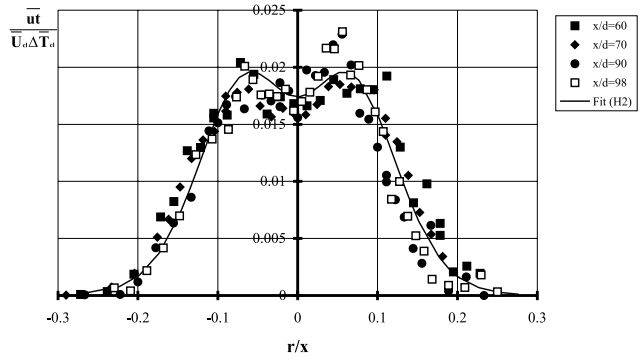

Fig. 26. $\overline{ut}$ normalised profiles, H6 case. H2 data fit using Eq. (B.2) with coefficients $a = 2.6769$, $b = -134.9451$, $c = -66.9745$.

$$\frac{\overline{u^2}}{\overline{U}_{\mathrm{cl}}^2} = a\left(\frac{r}{x}\right)^2 \mathrm{e}^{b(r/x)^2} + c\mathrm{e}^{d(r/x)^2}, \text{ also used for } t_{\mathrm{rms}}, \overline{ut}, \tag{B.2}$$

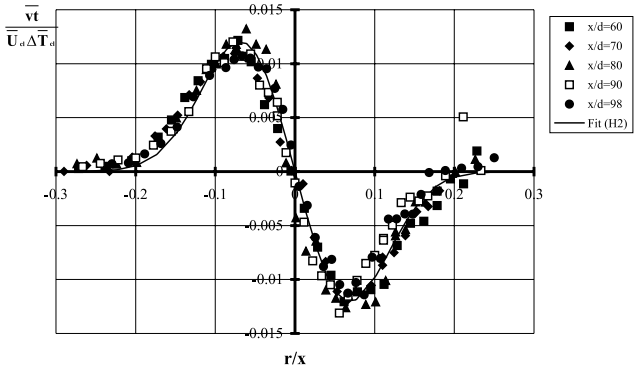

Fig. 27. $\overline{vt}$ normalised profiles, H6 case. H2 data fit using Eq. (B.4) with coefficients $a = 0.2771$, $b = -154.092$, $c = 2.1738$.

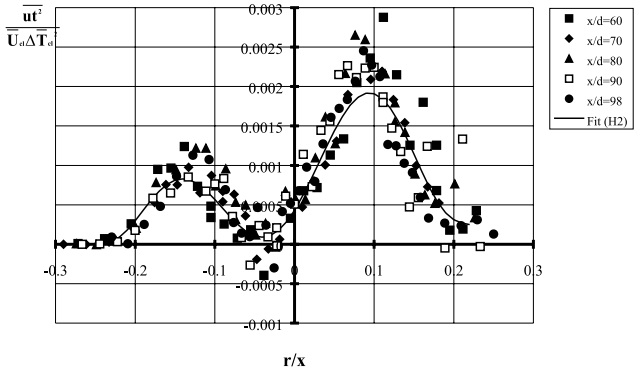

Fig. 28. $\overline{ut^2}$ normalised profiles, H6 case. H2 data fit using eighth-order polynomial, Eq. (B.8), with coefficients $a_1 = -1.2406\mathrm{e}3$, $a_2 = -2.338\mathrm{e}2$, $a_3 = 1.881\mathrm{e}2$, $a_4 = 2.982\mathrm{e}1$, $a_5 = -9.5993$, $a_6 = -1.2227$, $a_7 = 1.593\mathrm{e}-1$, $a_8 = 1.6181\mathrm{e}-2$, $a_9 = 4.2994\mathrm{e}-4$.

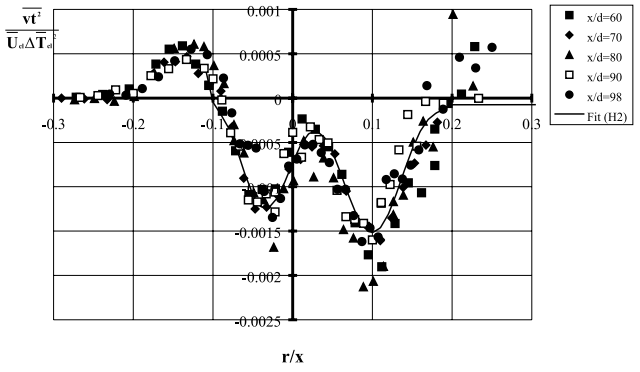

Fig. 29. $\overline{vt^2}$ normalised profiles, H6 case. H2 data fit using 10th-order polynomial, Eq. (B.8), with coefficients $a_1 = -8.585\mathrm{e}4$, $a_2 = -3.263\mathrm{e}5$, $a_3 = 2.0117\mathrm{e}5$, $a_4 = -2.428\mathrm{e}4$, $a_5 = -4.554\mathrm{e}3$, $a_6 = 8.62\mathrm{e}2$, $a_7 = 3.654\mathrm{e}1$, $a_8 = -8.7699$, $a_9 = -1.1583\mathrm{e}-1$, $a_{10} = 2.1684\mathrm{e}-2$, $a_{11} = -7.2683\mathrm{e}-4$.

$$\frac{\overline{v^2}}{\overline{U}_{\mathrm{cl}}^2} = a\mathrm{e}^{b(r/x)^c}, \tag{B.3}$$

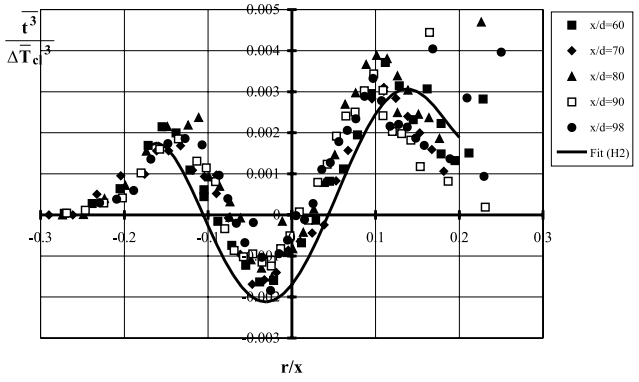

Fig. 30. $\overline{t^3}$ normalised profiles, H6 case. H2 data fitted using Eq. (B.8) with coefficients $a_1 = 56.2102$, $a_2 = 24.1383$, $a_3 = -9.8911$, $a_4 = -1.5107$, $a_5 = 0.3729$, $a_6 = 0.0263$, $a_7 = -0.0017$.

$$\frac{\overline{uv}}{\overline{U}_{cl}^2} = a\left(\frac{r}{x}\right)e^{b(r/x)^c}, \text{ also used for } \overline{vt}, \tag{B.4}$$

$$\frac{\overline{u^3}}{\overline{U}_{cl}^2} = a\left(\frac{r}{x}\right)^2 e^{b(r/x)^c} + de^{e(r/x)^2}, \tag{B.5}$$

$$\frac{\overline{u^2v}}{\overline{U}_{cl}^3} = a\left(\frac{r}{x}\right)^2 e^{b(r/x)^c} + d\left(\frac{r}{x}\right)e^{e(r/x)^2}, \tag{B.6}$$

$$\frac{\overline{uv^2}}{\overline{U}_{cl}^3} = a\left(\frac{r}{x}\right)^2 e^{b(r/x)^c} + de^{e(r/x)^f}, \tag{B.7}$$

nth-order polynomial fit given by

$$y = a_1x^n + a_2x^{n-1} + a_3x^{n-2} + \cdots + a_{n+1}. \tag{B.8}$$

For comparison with other heated jet conditions, an equation was fitted to the entire normalised data set for the H2 case. When calculating the kinetic energy and temperature variance budgets, curves were fitted to each axial location for better accuracy in calculating axial gradients.

References

Amielh, M., Djeridane, T., Anselmet, F., Fulachier, L., 1996. Velocity near-field of variable density turbulent jets. International Journal of Heat and Mass Transfer 39 (10), 2149–2164.

Anderson, S.M., 2000. Investigation of the flow field of a highly heated jet of air. Ph.D. Thesis. The University of Queensland, Australia.

Antonia, R.A., Prabhu, A., Stephenson, S.E., 1975. Conditionally sampled measurements in a heated turbulent jet. Journal of Fluid Mechanics 72, 455–480.

Antonia, R.A., Chambers, A.J., Hussain, A.K.M.F., 1980. Errors in the simultaneous measurements of temperature and velocity in the outer part of a heated jet. The Physics of Fluids 23 (5), 871–874.

Antonia, R.A., Browne, L.W.B., Chambers, A.J., Rajagopalan, S., 1983. Budget of the temperature variance in a turbulent plane jet. International Journal of Heat and Mass Transfer 26, 41–48.

Bashir, J., Uberoi, M., 1975. Experiments on turbulent structure and heat transfer in a two-dimensional jet. The Physics of Fluids 18 (4), 405–410.

Bremhorst, K., Anderson, S.M., 2001. Turbulent temperature measurements with cold wires: thermal, aerodynamic and asymmetry of multi-wire probe effects. In: Proceedings of ASME Sixth International Thermal Anemometry Symposium, Victoria University of Technology, Melbourne, Australia, 8–10 January 2001, Paper S285-IP2, 12 pp.

Bremhorst, K., Gehrke, P.J., 2000. Measured Reynolds stress distributions and energy budgets of a fully pulsed round air jet. Experiments in Fluids 28 (6), 519–531.

Bremhorst, K., Krebs, L., 1976. Reconsideration of constant current hot wire anemometers for the measurement of fluid temperature fluctuations. Journal of Physics E: Scientific Instrumentation 9 (10), 804–806.

Chevray, R., Tutu, N.K., 1978. Intermittency and preferential transport of heat in a round jet. Journal of Fluid Mechanics 88, 133–160.

Chen, C.J., Rodi, W., 1980. Vertical Turbulent Buoyant Jets a Review of Experimental Data. Pergamon Press, Great Britain.

Chua, L.P., Antonia, R.A., 1990. Turbulent Prandtl number in a circular jet. International Journal of Heat and Mass Transfer 33, 331–339.

Corrsin, S., Uberoi, M.S., 1949. Further experiments on the flow and heat transfer in a heated turbulent air jet. NACA TN 1865.

Dai, Z., Tseng, L.K., Faeth, G.M., 1995. Velocity/Mixture fraction statistics of round, self-preserving, buoyant turbulent plumes. Transactions of ASME, Journal of Heat Transfer 117, 918–926.

Gehrke, P.J., 1997. The turbulent kinetic energy balance of a fully pulsed axisymmetric jet. Ph.D. Thesis. The University of Queensland, Australia.

Gehrke, P.J., Bremhorst, K., 1993. Lateral velocity fluctuations and dissipation time-scale ratios for prediction of mean and fluctuating temperature fields. International Journal of Heat Mass Transfer 36 (7), 1943–1952.

Gharbi, A., Ruffin, E., Anselmet, F., Schiestel, R., 1996. Numerical modelling of variable density turbulent jets. International Journal of Heat and Mass Transfer 39 (9), 1865–1882.

Graham, L.J.W., Bremhorst, K., 1990. A linear compensation technique for inclined hot wire anemometers subjected to fluid temperature changes. Measurements Science and Technology 1, 13225.

Hussain, A.K.M.F., Ramjee, V., 1976. Effects of the axisymmetric contraction shape on incompressible turbulent flow. Journal of Fluid Engineering 95.

Lockwood, F., Moneib, H.A., 1980. Fluctuating temperature measurements in a heated round free jet. Combustion Science and Technology 22, 63–81.

Morkovin, M.V., 1962. Effects of compressibility on turbulent flow. In: Favre, A. (Ed.), The Mechanics of Turbulence, 367. Gordon and Breach, London.

Ogino, F., Takeuchi, H., Kudo, I., Mizushina, T., 1980. Heated jet discharged vertically into ambients of uniform and linear temperature profiles. International Journal of Heat and Mass Transfer 23, 1581–1588.

Panchapakesan, N.R., Lumley, J.L., 1993. Turbulence measurements in axisymmetric jets of air and helium.Part 2. Helium jet. Journal of Fluid Mechanics 246, 225–247.

Peterson, J., Bayazitoglu, Y., 1992. Measurements of velocity and turbulence in vertical axisymmetric isothermal and buoyant jets. Journal of Heat Transfer 114, 135–142.

Ruffin, E., Schiestel, R., Anselmet, F., Amielh, M., Fulachier, L., 1994. Investigation of characteristic scales in variable density turbulent jets using a second-order model. Physics of Fluids 6 (8), 2785–2799.

Sanders, H., Sarh, B., Gokalp, I., 1996. Etude numerique des jets turbulents a temperature elevee. Review of General Thermodynamics 35, 232–242.

Shih, T.H., Lumley, J.L., Janicka, J., 1987. Second-order modelling of a variable-density mixing layer. Journal of Fluid Mechanics 180, 93–116.

So, R.M.C., Aksoy, H., 1993. On vertical turbulent buoyant jets. International Journal of Heat and Mass Transfer 36 (13), 3187–3200.

Wilson, R.A.M., Danckwerts, P.V., 1964. Studies in turbulent mixing– II – a hot air jet. Chemical Engineering Science 19, 885–895.